Article

Strength Model for Prestressed Concrete Beams Subjected to Pure Torsion

Hyunjin Ju [1,*], Chanseo Jung [2] and Hae-Chang Cho [3]

1 School of Architecture and Design Convergence, Hankyong National University, Anseong 17579, Republic of Korea
2 Department of Architecture and Architectural Engineering, Hankyong National University, Anseong 17579, Republic of Korea; wjdckstj@hknu.ac.kr
3 Technology Center, Dream Structural Engineers Co., Ltd., Hwaseong 18471, Republic of Korea; hc.cho@dreamse.co.kr
* Correspondence: hju@hknu.ac.kr

Abstract: A torsional strength model for prestressed concrete beams was proposed considering the initial crack angle, principal stress angle, and longitudinal strain, which are affected by the axial stress induced by the effective prestress. The use of the torsional effective thickness was also proposed to calculate the torsional strength of prestressed concrete beams by considering the effect of prestress. The shear element in the torsional member was simplified under the assumption that the principal tensile stress and principal compressive strain were negligible in the ultimate state. The torsional strength was determined when the principal compressive stress or shear stress at the crack surface in the shear element reached the failure criterion according to the multipotential capacity model, which considers concrete crushing and aggregate interlocking as the main resistances to the applied load. The proposed strength model was verified using test specimens collected from existing experimental studies. The proposed model accurately evaluated the torsional strength of prestressed concrete beam specimens, regardless of the key variables of the prestressed concrete specimens, where the mean value of the tested results to the calculated torsional strengths was 1.123, and the corresponding coefficient of variation was 17.7% for 104 prestressed concrete beam specimens, while the ACI 318-19 torsional design method gave the mean and coefficient of variation of 0.880 and 24.3%, respectively.

Keywords: torsional strength; prestressed concrete; effective thickness; potential capacity; torsion test database

1. Introduction

Various types of irregular buildings have begun to appear with the development of construction materials and design techniques, requiring the consideration of complex load combinations [1–3]. In particular, structural members must be designed and analyzed considering the torsional moment, which has not been considered a major member force in the past. Precast concrete has been adopted in the construction of semiconductor factories, logistics warehouses, and knowledge industry centers because of its advantages, such as fast construction and excellent quality control, and efforts are being made to apply it to residential buildings [4–6]. The precast concrete method primarily involves prestressed concrete members that are formed by introducing an axial compression force to the cross-section of the concrete by prestressing tendons. Specifically, prestressed concrete members manufactured in a factory using the pre-tension method are assembled on-site and constructed with minimal formwork.

Figure 1a shows an example of such a precast concrete construction. The girder shown in the figure must resist normal shear forces and bending moments owing to the beams and slab, as well as torsional moments owing to the eccentricity caused by the slab members and beams. In addition, segmental box girders used in bridges are composed of prestressed

concrete members and can be subjected to torsional moments owing to eccentric loading, as shown in Figure 1b.
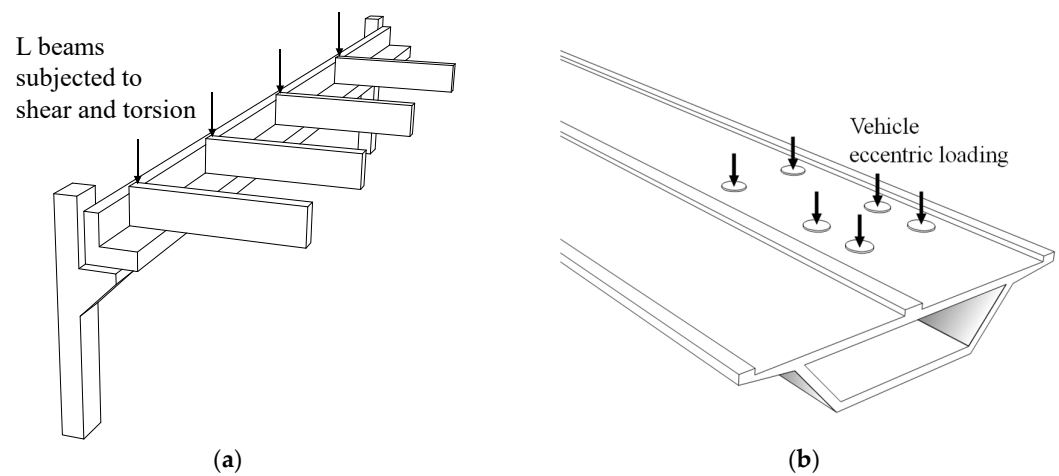
Figure 1. Prestressed concrete structures: (**a**) precast concrete structures; (**b**) segment-type precast concrete girder.

In this study, the behavioral mechanisms and failure modes of prestressed concrete members subjected to pure torsional moments were investigated, and a strength model was presented to lay the foundation for future torsion studies on prestressed concrete structures subjected to combined loads. In real practice, it is hard to find the concrete beams subjected to only a pure torsional moment. This study intended to provide some insight into the torsional behavior of prestressed concrete beams that should be investigated by carefully considering the favorable effect of prestress on concrete sections. In addition, the proposed method for prestressed concrete beams under pure torsion could be expanded to cases of combined loads, including bending, shear, and axial force, as well as torsion, in the future study.

The proposed torsional strength model considers the initial crack angle, principal stress angle, torsional effective thickness, and longitudinal strain, which are affected by the axial stress induced by the effective prestress. In addition, the torsional strength is determined by capacities of concrete crushing or aggregate interlocking at the crack surface. The model will be verified using test specimens collected from existing experimental studies, and the effect of key variables will be discussed.

## 2. Torsional Strength Model for Prestressed Concrete Beams

In our previous work, a nonlinear analysis model was developed to evaluate the torsional behavior [7], and multipotential capacity criteria were proposed to rationally evaluate the capacity of reinforced concrete beams to resist torsion along with bending, shear, and axial forces [8,9]. In addition, it has been expanded to a torsional strength model for steel fiber-reinforced concrete beams with transverse reinforcement [10]. A rectangular section of reinforced concrete was idealized as a panel element with a torsional effective thickness, and the strength of the member was determined at the point where the stress acting on each panel element reached the multipotential capacity criterion, which is defined as the resistance by aggregate interlocking, compressive failure of concrete, and spalling failure of the concrete section outside the closed stirrups. Based on this model, a torsional strength evaluation model for reinforced concrete (RC) beams under combined loading was established [3], and a model for estimating the pure torsional strength of prestressed concrete beams was presented.

2.1. Assumptions and Shear Element

In this study, a torsional strength model for prestressed concrete beams based on thin-walled tube theory [11] and a softened truss model [12] are presented. According to the thin-walled tube theory, the torsional moment (T) acting on a reinforced concrete beam is resisted by the shear flow (q) within the concrete thin-walled tube defined by its effective thickness (t_d) [13–15]. The shear flow (q) is characterized by the shear stress (τ_{lt}) in the concrete thin-walled tube defined by the effective thickness (t_d), as shown in Figure 2. The torsional moment (T) is calculated using the area enclosed by the centerline of the shear flow (A_o) as follows:

$$T = 2A_o q = 2A_o t_d \tau_{lt} \tag{1}$$

The relationship between the torsional moment (T) and variables (t_d, A_o) in Equation (1) can be compared to the relationship between the bending moment (M), neutral axis depth (c), and moment arm length (jd) [16]. Thus, just as the bending moment can be easily estimated if the neutral axis depth is known from the force equilibrium, the torsional moment acting on the cross-section (T) can be easily estimated if the torsional effective thickness (t_d) is determined.
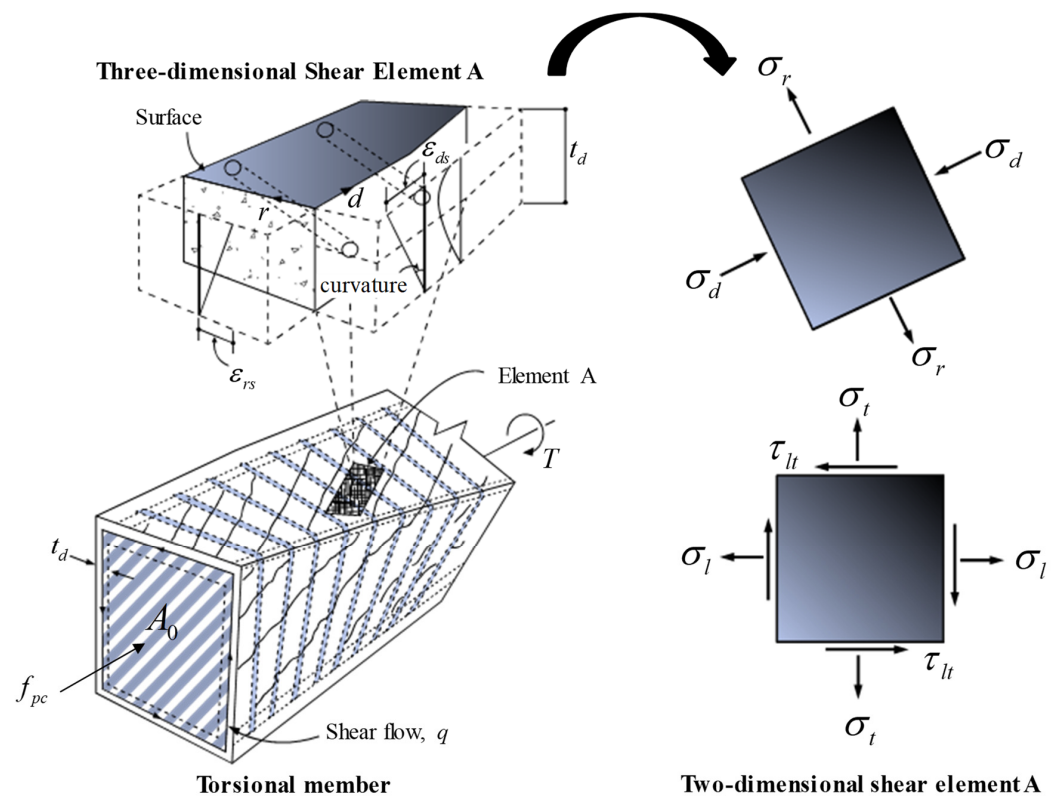
Figure 2. Prestressed concrete beam under pure torsion.

Meanwhile, as the axial strain in a concrete member increases, the crack width increases, which weakens aggregate interlocking, one of the factors in shear resistance [17]. This behavioral mechanism is referred to as the strain effect and is considered the main variable determining the shear capacity of concrete members in the modified compression field theory (MCFT) [18]. The torsional strength model presented in this study also considers the strain effect in the concrete cross-section as the main resistance mechanism. In this model, a member is idealized as a shear element with an effective thickness, and the stresses in the element are calculated to determine the strength by considering the multipotential capacity criteria. The longitudinal reinforcement and prestressing tendons are assumed to be symmetrically located around the center of the prestressed concrete cross-section, resisting pure torsion.

The equilibrium equations in the longitudinal, transverse, and shear directions of the shear element in a thin-walled tube with an effective thickness were obtained from Mohr's stress circles [13] as follows:

$$\sigma_l = \sigma_d cos^2\alpha_1 + \sigma_r sin^2\alpha_1 + \rho_l f_l + \rho_p \Delta f_p + f_{pc} \tag{2}$$

$$\sigma_t = \sigma_d sin^2\alpha_1 + \sigma_r cos^2\alpha_1 + \rho_t f_t \tag{3}$$

$$\tau_{lt} = (\sigma_r - \sigma_d)sin\alpha_1 cos\alpha_1 \tag{4}$$

It was assumed that the prestressed tension was applied only in the longitudinal direction. Here, σ_l is the normal stress in the longitudinal direction, as shown in Figure 2; σ_t is the normal stress in the longitudinal direction; τ_{lt} is the shear stress in the $l - t$ coordinate system; σ_d and σ_r are the principal compressive and tensile stresses, respectively; and α_1 is the principal stress angle, which is defined as the angle between the longitudinal axis and the principal compressive direction. f_l and f_t are the stresses in the longitudinal and transverse reinforcements, respectively, and ρ_l and ρ_t are the longitudinal and transverse reinforcement ratios, respectively, defined as $A_l/(t_d p_o)$ and $A_t/(t_d s)$. Here, A_l is the cross-sectional area of the longitudinal reinforcement; A_t is the cross-sectional area of a closed stirrup leg in the transverse direction; p_o is the perimeter enclosed by the shear flow; and s is the spacing of the closed stirrups. ρ_p is the reinforcement ratio of the prestressing tendons, defined as $A_p/(t_d p_o)$, and Δf_p is the stress increased by the torsional moment in addition to the effective prestress (f_{pe}) in the prestressing tendon. It is assumed that all stresses increase in the prestressing tendons owing to the torsional moment occurring within the thickness of the thin wall, and the stress in the concrete section caused by the effective prestress (f_{pc}) is calculated by considering the area enclosed by the outer perimeter (A_{cp}) in the concrete section as follows:

$$f_{pc} = A_p f_{pe}/A_{cp} \tag{5}$$

For simplicity in Equation (5), the cross-sectional area owing to the reinforcement and prestressing tendons cannot be excluded from the gross cross-sectional area.

Similar to the force equilibrium, the strain compatibilities in the longitudinal (ε_l), transverse (ε_t), and principal (ε_d and ε_r) directions are obtained from Mohr's strain circle as follows:

$$\varepsilon_l + \varepsilon_t = \varepsilon_d + \varepsilon_r \tag{6}$$

Because the magnitudes of the principal tensile stress (σ_r) and principal compressive strain (σ_d) are quite small at the ultimate state, the equilibrium and strain compatibility equations are simplified, as shown in Mohr's circle in Figure 3, by assuming $\sigma_r = 0$ and $\varepsilon_d = 0$, which gives

$$\sigma_l = \sigma_d cos^2\alpha_1 + \rho_l f_l + \rho_p \Delta f_p + f_{pc} \tag{7}$$

$$\sigma_t = \sigma_d sin^2\alpha_1 + \rho_t f_t \tag{8}$$

$$\tau_{lt} = -\sigma_d sin\alpha_1 cos\alpha_1 \tag{9}$$

$$\varepsilon_r = \varepsilon_l + \varepsilon_t \tag{10}$$

In addition, the normal stress in the transverse direction (σ_t) can be considered zero when there is no clamping force, and the principal compressive stress and stress of the reinforcement in the transverse direction can be expressed as follows:

$$\sigma_d = \frac{-\tau_{lt}}{sin\alpha_1 cos\alpha_1} \tag{11}$$

$$f_t = \frac{-\sigma_d sin^2\alpha_1}{\rho_t} \tag{12}$$

The shear stress at the crack surface (τ_{21}^c) can be calculated from the simplified Mohr stress circle shown in Figure 3a as follows:

$$\tau_{21}^c = \sigma_d sin\beta cos\beta \tag{13}$$

This was considered to be the resistance caused by aggregate interlocking. Here, β is the difference between the initial crack angle (α_2) and principal stress angle (α_1), which is calculated as follows:

$$\beta = \alpha_2 - \alpha_1 \tag{14}$$

If no compressive force acts along the member axis, the initial crack angle (α_2) can be assumed to be 45°. However, if a member is subjected to compressive forces in the longitudinal direction, such as a preload or prestress, a value less than 45° should be considered for the initial crack angle (α_2) [19,20].
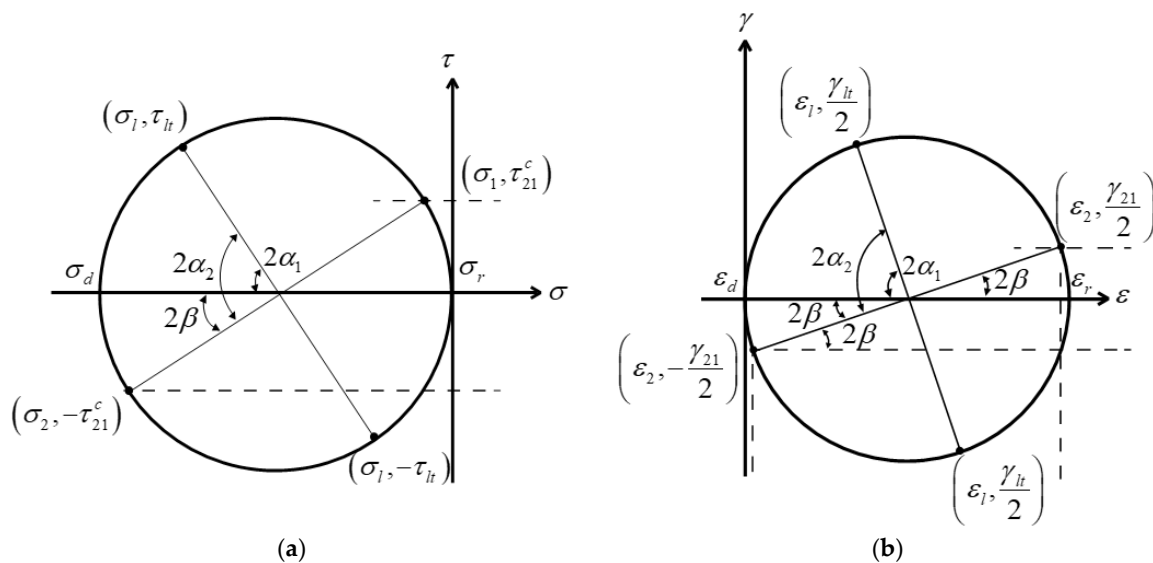
Figure 3. Assumed Mohr's circles: (**a**) stress; (**b**) strain.

The torsional effective thickness of a thin-walled tube (t_d) is an important variable for determining the torsional strength. Based on the analytical results of reinforced concrete beams subjected to pure torsional moments, Ju et al. [21] developed an expression for the effective thickness at the ultimate state as a function of the concrete compressive strength (f_c') and reinforcement ratios in the longitudinal and transverse directions ($\rho_L = A_l / A_{cp}$ and $\rho_T = A_t p_h / (A_{cp} s)$) as follows:

$$t_d = 10.6 \frac{A_{cp}}{p_c} \left(\frac{\rho_L + \rho_T}{f_c'} \right)^{0.42} \geq 0.75 A_{cp} / p_c \tag{15}$$

where p_c is the outer perimeter of the concrete cross-section. Because the torsional effective thickness (t_d) is determined by the force equilibrium in the concrete and the reinforcement in the thin-walled tube [22–24], the effective thickness (t_d) of a prestressed concrete beam must be adjusted to consider the effect of prestress.

2.2. Effect of Prestress

Because prestressed concrete beams are subjected to compressive forces owing to prestressing along the axis of the member, the initial crack angle is calculated by considering the prestressing stress (f_{pc}) at the center of the cross-section as follows [8,25]:

$$\alpha_2 = 0.5 atan \left(\frac{2\tau_{cr}}{f_{pc}} \right) \tag{16}$$

The compressive stress in the concrete section due to prestress (f_{pc}) is taken as positive. Here, τ_{cr} is the cracking shear stress, which is calculated from Mohr's stress circles in an elastic state as follows:

$$\tau_{cr} = f_{cr}\sqrt{1 + \frac{f_{pc}}{f_{cr}}} \tag{17}$$

where f_{cr} is the crack shear strength without the effect of prestress and is taken as $0.33\sqrt{f_c'}$ [26].

The principal stress angle (α_1) is an important factor in determining the contribution of reinforcement in both directions to the torsional strength using the space truss model [22,27], as well as the shear stress (τ_{21}^c) at the crack surface, as shown in Equations (13) and (14), where the principal stress angle (α_1) is determined by the longitudinal and transverse reinforcement ratios and their stresses. Ju et al. [21] analyzed reinforced concrete beams resisting pure torsion using the softened truss model proposed by Jeng and Hsu [28] and derived a formula for the principal stress angle (α_1) at the ultimate states. However, this equation is derived from the regression of the analysis results for reinforced concrete beams and limits the minimum principal stress angle to $36°$. Therefore, it is not suitable for prestressed concrete beams, in which the principal stress angle is significantly lower than that of reinforced concrete members. In this study, based on the force equilibrium and considering the contribution of the prestressing tendon, the suggested principal stress angle is as follows:

$$\alpha_1 = \cot^{-1}\left(\sqrt{\frac{A_l f_{ly} + A_p f_{pe}}{A_t f_{ty}}\frac{s}{p_h}}\right) \tag{18}$$

where p_h is the length enclosed by the centerline of the vertical reinforcement. The yield stresses of the longitudinal and transverse reinforcements (f_{ly} and f_{ty}) were considered, and the effective prestress was used instead of assuming the yield of the prestressing tendon to avoid obtaining excessively low angles caused by the prestress. In addition, as in ACI 318-19 [29], the minimum value of the principal stress angle was limited to $30°$.

The strain effect was reflected by calculating the longitudinal strain owing to the prestress and torsional moment. The longitudinal force due to torsion is relieved by the effective prestressing force introduced, which is resisted by the reinforcement and prestressing tendon in the cracked cross-section. Therefore, the longitudinal strain (ε_l) was calculated as follows:

$$\varepsilon_l = \frac{T p_o \cot\alpha_1 / 2A_o - A_p f_{pe}}{E_l A_l + E_p A_p} \tag{19}$$

where E_l and E_p are the moduli of elasticity of the longitudinal reinforcement and prestressing tendon, respectively, and A_l and A_p are the cross-sectional areas of the longitudinal reinforcement and prestressing tendon, respectively.

The material models for the steel rebar and prestressing tendon are as follows, respectively:

$$f_s = E_s \varepsilon_s \leq f_y + E_{sp}(\varepsilon_s - f_y/E_s) \tag{20}$$

$$f_p = E_p \varepsilon_p \left[1 + \left(\frac{E_p \varepsilon_p}{f_{pu}}\right)^5\right]^{\frac{1}{5}} \tag{21}$$

where f_s and f_p are the stresses in the reinforcement and prestressing tendons, respectively, and E_{sp} is the post-yield modulus of the reinforcement, which is considered $0.01E_s$. In addition, f_y and f_{pu} are the yield stresses in the reinforcement and prestressing tendons, respectively, and ε_s and ε_p are the strains in the reinforcement and prestressing tendons, respectively.

The effective thickness of the prestressed concrete beam in the ultimate state ($t_{d,psc}$) should reflect the effect of prestress, which is suggested based on the effective thickness calculation formula in Equation (15), and the exponent is simplified to 0.4 as follows:

$$t_{d,psc} = 10.6\frac{A_{cp}}{p_c}\left(\frac{\rho_L + \rho_T + \rho_p\left(f_{py}/f_y\right)}{f_c{}'}\right)^{0.4} \geq 0.75 A_{cp}/p_c \tag{22}$$

The effective thickness was limited to $0.75 A_{cp}/p_c$, which is the effective thickness before cracking, as specified in ACI 318-19 [29].

2.3. Multipotential Capacity

According to the existing experimental results, the reinforcement reaches the yield strain before the reinforced concrete member reaches the ultimate torsional strength, which is determined by the compressive strength of the concrete. Thus, the existing analytical models define the ultimate state of reinforced concrete beams subjected to torsion at the compressive failure of the concrete [13,22,27]. On the other hand, Ju et al. [3,8,9,21] proposed multipotential capacity criteria to define the torsional strength of reinforced concrete members, in which the torsional strength is governed by the compressive failure of concrete, the resistance of the aggregate interlock, or spalling failure that may occur in the outer concrete section of closed stirrups when the concrete cover thickness is excessive, as shown in Figure 4. However, spalling failure has been reported to occur when the cover is significantly thick, and spalling may occur beyond the ultimate strength [30,31]. Therefore, it is hypothesized that failure occurs at the point where the principal compressive stress (σ_d) developed within the member reaches the maximum compressive strength of the concrete (σ_{cap}^c), or the shear stress (τ_{21}^c) developed at the crack faces in the web of the concrete reaches the resistance of the aggregate interlock (τ_{cap}^c) when a reinforced concrete member resists loading, including torsion. The principal compressive stress (σ_d) in the member and the shear stress (τ_{21}^c) at the crack surface were calculated using Equations (11) and (13), respectively, and the maximum compressive strength (σ_{cap}^c) and resistance of the aggregate interlock (τ_{cap}^c) are calculated as follows:

$$\sigma_{cap}^c = \zeta f_c{}' \tag{23}$$

$$\tau_{cap}^c = \frac{0.18\lambda\sqrt{f_c{}'}}{0.31 + \frac{21 w_s}{a_{g,max}}} \tag{24}$$

where ζ is the concrete softening coefficient, which is taken as $1/(0.8 + 170\varepsilon_r)$, λ is the lightweight aggregate modulus (1.0) for normal weight concrete and 0.75 for lightweight aggregate concrete, $a_{g,max}$ is the maximum size of the aggregate, and $a_{g,max} - 0.16 f_c{}'$ is used for high-strength concrete above 40 MPa. The aggregate interlock resistance in Equation (24) is defined as a function of the shear crack width (w_s), which is multiplied by the average shear crack spacing ($s_{m\theta}$) and tensile strain at the crack surface (ε_1) as follows:

$$w_s = s_{m\theta}\varepsilon_1 \tag{25}$$

The tensile strain at the crack surface (ε_1) can be obtained from the Mohr's strain circle as follows:

$$\varepsilon_1 = \varepsilon_r cos^2\beta \tag{26}$$

The average shear crack spacing ($s_{m\theta}$) was determined based on the equation suggested by Ju et al. [3] for reinforced concrete beams, which considered the effect of prestress as follows:

$$s_{m\theta} = \frac{1500}{25\sqrt{\rho_L + \rho_p\left(f_{py}/f_y\right)} + 45\sqrt{\rho_T}} \leq \text{member height} \tag{27}$$

Here, a new term of $\rho_p\left(f_{py}/f_y\right)$ is introduced for the crack control capability due to the prestressing tendon.
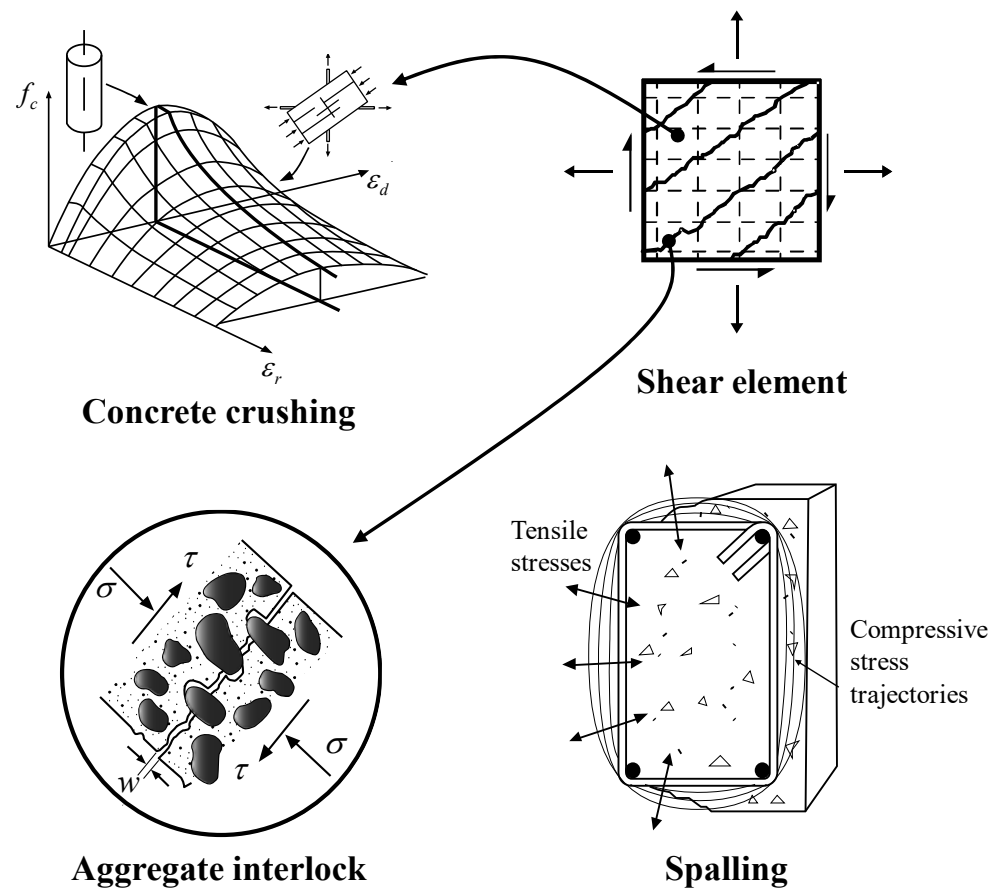
Figure 4. Failure criteria of the multipotential capacity.

2.4. Calculation Procedure for Torsional Strength

The procedure for calculating the torsional strength of the prestressed concrete members is illustrated in Figure 5. The calculation procedure was conducted by increasing the torsional moment in a load-controlled manner, calculating the stresses and strains in the shear elements, and then determining the torsional strength at the point where the multipotential capacity was reached as follows.

1. Considering the assumed torsional moment acting on a given section with material properties, the shear stress (τ_{lt}) due to torsion (T) is calculated using Equation (1). The torsional effective thickness (t_d) is calculated using Equation (22) to determine the A_o ($= A_c - 0.5p_h t_d + t_d^2$). The average shear crack spacing ($s_{m\theta}$), initial crack angle (α_2), and principal stress angle (α_1) are calculated using Equations (27), (16), and (18).
2. Estimation of stresses and strains in the shear element. The principal compressive stress (σ_d) and shear stress (τ_{21}^c) at the crack surface are calculated using Equations (11) and (13), respectively, and the longitudinal strain (ε_l) and transverse strain (ε_t) are calculated using Equations (19) and (20), respectively.
3. The torsional strength of the member is then determined by checking whether the previously calculated principal compressive stress (σ_d) and shear stress at the crack surface (τ_{21}^c) reached the compressive failure (σ_{cap}^c) and aggregate engagement failure criteria (τ_{cap}^c) in Equations (23) and (24), respectively.
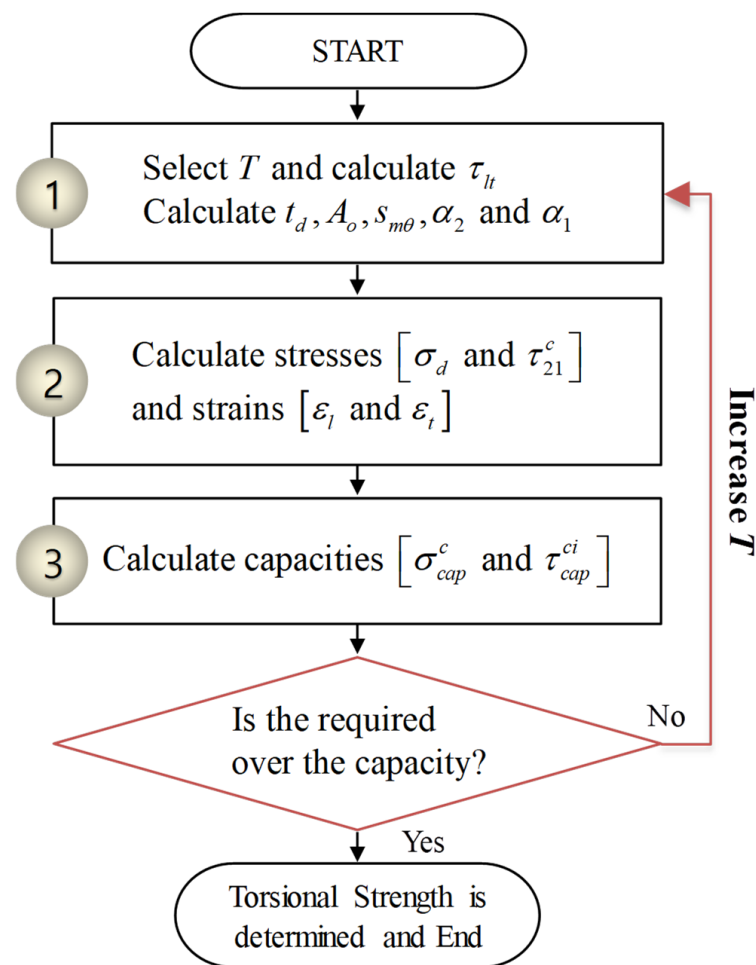
Figure 5. Calculation procedure of the proposed strength model.

If the stresses do not meet the failure criteria, return to step 1, increase the magnitude of the torsional moment, and repeat steps 1–3 until one of the failure criteria is satisfied.

3. Verification of the Proposed Model

3.1. Experimental Data of Prestressed Concrete Beams Subjected to Pure Torsion

To verify the torsional strength model, 104 prestressed concrete beam specimens subjected to pure torsion were collected from the existing literature [30,32–38] and are listed in Table 1. All the collected specimens were symmetrically reinforced with longitudinal reinforcing bars (A_l) and prestressing tendons (A_p) at approximately the center of the cross-section, and the distributions of the compressive strength and reinforcement ratios in the concrete cross-section are shown in Figure 6. The concrete compressive strength of the experimental specimens (f_c') ranged from 28.6 to 95.6 MPa, and the reinforcement ratios in the longitudinal (ρ_L) and transverse directions (ρ_T) ranged from 0 to 3.91% and 0.42% to 2.05%, respectively. In addition, the prestressing reinforcement ratio (ρ_p) varied from 0 to 2.3%, and the compressive stress in the concrete section caused by the effective prestress (f_{pc}) varied from 0 to 19.75 MPa. The longitudinal reinforcement ratio ($\rho_L f_{ly}$) was larger than the transverse reinforcement ratio ($\rho_T f_{ty}$) for most of the experimental specimens, and the reinforcement ratio in the longitudinal direction was larger owing to the prestressing tendons. The collected specimens included four non-prestressed concrete beams from Mitchell et al. [37], which were used to compare the torsional strength of reinforced concrete according to the prestress in the concrete section (f_{pc}).

Table 1. Database of prestressed concrete beam specimens subjected to pure torsion.

Author	Beam Name	f_{ck} (MPa)	f_{ly} (MPa)	E_{sl} (MPa, ×10⁵)	f_{py} (MPa)	E_{ps} (MPa, ×10⁵)	f_{ty} (MPa)	E_{st} (MPa, ×10⁵)	B (mm)	H (mm)	A_l (mm²)	A_{ps} (mm²)	f_{pe} (Mpa)	A_t (mm²)	x_0 (mm)	y_0 (mm)	s (mm)	T_{cr} (kNm)	T_u (kNm)
Mitchell et al. (1974) [16]	PT4 *	28.61	424.03	2.00	0	0.00	328	2.00	381.0	381	1600.00	0.00	0.00	71.00	346.2	346.2	101.6	-	65.42
	PT5 *	33.78	424.03	2.00	0	0.00	328	2.00	355.6	355.6	1600.00	0.00	0.00	71.00	342.9	342.9	101.6	-	57.62
	PT6 *	32.54	424.03	2.00	0	0.00	328	2.00	431.8	431.8	1600.00	0.00	0.00	71.00	342.9	342.9	101.6	-	64.40
	P1	32.27	327.50	2.00	1475	1.97	328	2.00	355.6	431.8	570.40	462.96	1144.25	71.00	320.8	397.0	96.5	-	81.91
	P2 *	32.89	327.50	2.00	1475	1.97	328	2.00	355.6	431.8	570.40	462.96	1162.89	71.00	320.8	397.0	96.5	-	86.21
	P3	33.99	327.50	2.00	1475	1.97	328	2.00	355.6	431.8	427.80	115.74	1140.93	71.00	320.8	397.0	96.5	-	53.10
	P4 *	31.72	327.50	2.00	1475	1.97	328	2.00	355.6	431.8	570.40	462.96	1143.70	71.00	320.8	397.0	96.5	-	85.42
	P5	38.89	0.00	0.00	1475	1.97	328	2.00	355.6	431.8	0.00	1543.20	1143.25	71.00	320.8	397.0	96.5	-	97.73
	P6	38.89	379.21	1.97	0	0.00	328	2.00	355.6	431.8	6000.00	0.00	0.00	71.00	320.8	397.0	96.5	-	88.13
Chander et. al. (1970) [34]	C/1	38.36	335.77	2.00	1855	1.94	335	2.00	101.6	304.8	285.20	198.06	594.25	31.67	69.9	273.1	101.6	5.87	6.70
	E/2 **	38.36	335.77	2.00	1855	1.94	335	2.00	101.6	304.8	285.20	198.06	608.04	31.67	69.9	273.1	101.6	5.36	5.97
	C/3	36.17	335.77	2.00	1855	1.94	335	2.00	101.6	304.8	285.20	198.06	719.66	31.67	69.9	273.1	76.2	7.85	8.93
	E/4 **	36.17	335.77	2.00	1855	1.94	335	2.00	101.6	304.8	285.20	198.06	775.65	31.67	69.9	273.1	76.2	6.15	7.31
	C/5	40.40	335.77	2.00	1855	1.94	335	2.00	101.6	304.8	285.20	297.10	974.52	31.67	69.9	273.1	101.6	8.52	8.54
	E/6 **	40.40	335.77	2.00	1855	1.94	335	2.00	101.6	304.8	285.20	297.10	974.52	31.67	69.9	273.1	101.6	7.43	7.93
	C/9	38.53	335.77	2.00	1855	1.94	335	2.00	101.6	304.8	285.20	297.10	977.38	31.67	69.9	273.1	76.2	8.54	9.62
	E/10 **	38.53	335.77	2.00	1855	1.94	335	2.00	101.6	304.8	285.20	297.10	977.38	31.67	69.9	273.1	76.2	8.51	9.00
	C/11	45.84	335.77	2.00	1855	1.94	335	2.00	101.6	304.8	285.20	594.19	852.57	31.67	69.9	273.1	101.6	10.27	10.68
	E/12 **	45.84	335.77	2.00	1855	1.94	335	2.00	101.6	304.8	285.20	594.19	852.57	31.67	69.9	273.1	101.6	10.33	10.42
	C/15	48.00	335.77	2.00	1855	1.94	335	2.00	101.6	304.8	285.20	594.19	901.34	31.67	69.9	273.1	76.2	12.02	12.02
	E/16 **	48.00	335.77	2.00	1855	1.94	335	2.00	101.6	304.8	285.20	594.19	901.34	31.67	69.9	273.1	76.2	12.02	12.18
	C/7	37.67	335.77	2.00	1855	1.94	335	2.00	101.6	228.6	285.20	396.13	973.81	31.67	69.9	196.9	101.6	6.16	6.19
	E/8 **	37.67	335.77	2.00	1855	1.94	335	2.00	101.6	228.6	285.20	396.13	973.81	31.67	69.9	196.9	101.6	5.11	5.70
	C/13	43.53	335.77	2.00	1855	1.94	335	2.00	101.6	228.6	285.20	198.06	1016.43	31.67	69.9	196.9	101.6	6.17	6.68
	E/14 **	43.53	335.77	2.00	1855	1.94	335	2.00	101.6	228.6	285.20	198.06	1016.43	31.67	69.9	196.9	101.6	6.46	6.99
	C/17	34.38	335.77	2.00	1855	1.94	335	2.00	101.6	228.6	285.20	99.03	1023.75	31.67	69.9	196.9	101.6	3.93	4.64
	E/18 **	34.38	347.50	2.00	1855	1.94	335	2.00	101.6	228.6	285.20	99.03	1023.75	31.67	69.9	196.9	101.6	4.06	4.67
	C/19	35.45	347.50	2.00	1855	1.94	335	2.00	101.6	228.6	285.20	396.13	1158.18	31.67	69.9	196.9	101.6	5.34	5.83
	E/20 **	35.45	393.00	2.00	1855	1.94	335	2.00	101.6	228.6	285.20	396.13	1158.18	31.67	69.9	196.9	101.6	5.77	6.00
	SP1261	34.51	348.19	2.00	1855	1.94	359	2.00	152.4	304.8	506.80	396.13	1198.31	71.30	117.5	269.9	101.6	16.85	18.63
	SP1262	34.51	393.00	2.00	1855	1.94	399	2.00	152.4	304.8	285.20	396.13	1198.31	31.67	120.7	273.1	101.6	11.74	15.21

Table 1. *Cont.*

Author	Beam Name	f_{ck} (MPa)	f_{ly} (MPa)	E_{sl} (MPa, $\times10^5$)	f_{py} (MPa)	E_{ps} (MPa, $\times10^5$)	f_{ty} (MPa)	E_{st} (MPa, $\times10^5$)	B (mm)	H (mm)	A_l (mm²)	A_{ps} (mm²)	f_{pe} (Mpa)	A_t (mm²)	x_0 (mm)	y_0 (mm)	s (mm)	T_{cr} (kNm)	T_u (kNm)
Chander et. al. (1970) [34]	SP1263	38.96	348.19	2.00	1855	1.94	359	2.00	152.4	304.8	506.80	396.13	1172.14	71.30	117.5	269.9	101.6	16.43	19.79
	SP1264	38.96	393.00	2.00	1855	1.94	399	2.00	152.4	304.8	285.20	396.13	1172.14	31.67	120.7	273.1	101.6	13.58	15.38
	SP1269	34.20	334.40	2.00	1855	1.94	356	2.00	152.4	304.8	506.80	396.13	724.71	71.30	117.5	269.9	101.6	15.95	17.08
	SP1270	34.20	368.18	2.00	1855	1.94	411	2.00	152.4	304.8	285.20	396.13	724.71	31.67	120.7	273.1	101.6	14.68	14.68
	SP1271	33.89	334.40	2.00	1855	1.94	356	2.00	152.4	304.8	506.80	396.13	728.46	71.30	117.5	269.9	101.6	16.43	18.35
	SP1272	33.89	368.18	2.00	1855	1.94	411	2.00	152.4	304.8	285.20	396.13	728.46	31.67	120.7	273.1	101.6	12.64	13.68
	SPEC I	40.97	368.18	2.00	1855	1.94	411	2.00	152.4	304.8	285.02	396.13	874.32	31.67	120.7	273.1	101.6	17.19	17.19
	SPEC II	40.97	368.18	2.00	1855	1.94	411	2.00	152.4	304.8	285.02	396.13	874.32	31.67	120.7	273.1	101.6	14.52	16.12
	SP1267	34.95	4334.40	2.00	1855	1.94	356	2.00	152.4	304.8	506.71	396.13	1174.14	71.26	117.5	269.9	101.6	18.16	19.12
	SP1241	33.41	368.18	2.00	1855	1.94	419	2.00	101.6	304.8	285.02	198.06	1172.76	31.67	69.9	273.1	101.6	8.58	9.37
	SP1242	33.41	368.18	2.00	1855	1.94	419	2.00	101.6	304.8	285.02	198.06	1172.76	31.67	69.9	273.1	101.6	8.43	9.20
	SPC1243	36.54	368.18	2.00	1855	1.94	405	2.00	101.6	304.8	285.02	198.06	600.20	31.67	69.9	273.1	101.6	6.63	8.02
	SPE1244 **	36.54	368.18	2.00	1855	1.94	405	2.00	101.6	304.8	285.02	198.06	600.20	31.67	69.9	273.1	101.6	6.63	7.54
	SPC1245	40.20	393.00	2.00	1855	1.94	394	2.00	101.6	304.8	285.02	594.19	891.15	31.67	69.9	273.1	101.6	11.05	11.64
	SPE1246 **	40.20	393.00	2.00	1855	1.94	394	2.00	101.6	304.8	285.02	594.19	891.15	31.67	69.9	273.1	101.6	9.47	10.96
	SP1247	37.47	393.00	2.00	1855	1.94	394	2.00	101.6	304.8	285.02	297.10	1004.09	31.67	69.9	273.1	101.6	8.77	10.59
	SPC941	33.81	393.00	2.00	1855	1.94	405	2.00	101.6	228.6	285.02	99.03	1014.50	31.67	69.9	196.9	101.6	5.33	5.90
	SPE942 **	33.81	393.00	2.00	1855	1.94	405	2.00	101.6	228.6	285.02	99.03	1014.50	31.67	69.9	196.9	101.6	4.54	5.05
Mukherjee et al. (1967) [38]	SP1	39.02	351.63	2.00	896	2.00	400	2.00	152.4	304.8	285.02	535.00	745.90	31.67	120.7	273.1	76.2	15.46	21.56
	SP2	43.45	351.60	2.00	896	2.00	400	2.00	152.4	304.8	285.02	535.00	791.40	31.67	120.7	273.1	101.6	17.34	19.32
	SP3	48.05	317.17	2.00	896	2.00	352	2.00	152.4	304.8	791.73	535.00	822.53	71.26	117.5	269.9	76.2	18.85	26.42
	SP4	45.20	313.03	2.00	896	2.00	352	2.00	152.4	304.8	506.71	535.00	815.95	71.26	117.5	269.9	101.6	18.51	22.44
	SP5	45.12	313.03	2.00	896	2.00	352	2.00	152.4	304.8	506.71	535.00	815.95	71.26	117.5	269.9	127.0	18.17	22.69
	SP6	42.89	423.08	2.00	896	2.00	400	2.00	152.4	304.8	285.02	283.00	935.92	31.67	120.7	273.1	76.2	14.46	17.29
	SP7	46.51	363.50	2.00	896	2.00	400	2.00	152.4	304.8	285.02	283.00	951.76	31.67	120.7	273.1	101.6	16.38	17.63
	SP8	45.73	302.48	2.00	896	2.00	370	2.00	152.4	304.8	791.73	283.00	946.10	71.26	117.5	269.9	76.2	16.38	21.02
	SP9	44.33	336.13	2.00	896	2.00	370	2.00	152.4	304.8	506.71	283.00	949.50	71.26	117.5	269.9	101.6	16.04	20.90
	SP10	40.89	336.13	2.00	896	2.00	370	2.00	152.4	304.8	506.71	283.00	921.21	71.26	117.5	269.9	127.0	16.38	20.11
	SP11	41.38	423.06	2.00	896	2.00	400	2.00	152.4	304.8	285.02	1070.00	740.22	31.67	120.7	273.1	76.2	23.39	23.39
	SP12	41.22	423.06	2.00	896	2.00	400	2.00	152.4	304.8	285.02	1070.00	735.43	31.67	120.7	273.1	101.6	23.16	23.16
	SP13	46.83	293.58	2.00	896	2.00	423	2.00	152.4	304.8	791.73	1070.00	807.86	71.26	117.5	269.9	76.2	25.42	26.21

Table 1. *Cont.*

Author	Beam Name	f_{ck} (MPa)	f_{ly} (MPa)	E_{sl} (MPa, ×10⁵)	f_{py} (MPa)	E_{ps} (MPa, ×10⁵)	f_{ty} (MPa)	E_{st} (MPa, ×10⁵)	B (mm)	H (mm)	A_l (mm²)	A_{ps} (mm²)	f_{pe} (Mpa)	A_t (mm²)	x_0 (mm)	y_0 (mm)	s (mm)	T_{cr} (kNm)	T_u (kNm)
	SP14	49.10	336.12	2.00	896	2.00	370	2.00	152.4	304.8	506.71	1070.00	817.44	71.26	117.5	269.9	101.6	25.76	26.21
	SP15	38.53	305.09	2.00	896	2.00	423	2.00	152.4	304.8	506.71	1070.00	702.80	71.26	117.5	269.9	127.0	22.26	22.94
	PA1	44.30	435.00	2.00	1638	2.05	310	2.00	254.0	254	285.20	92.80	1103.00	32.00	222.0	222.0	65.0	18.71	22.72
	PA1R	43.60	435.00	2.00	1638	2.05	310	2.00	254.0	254	285.20	92.80	1109.00	32.00	222.0	222.0	65.0	18.57	21.75
	PA2	45.60	483.00	2.00	1663	2.05	310	2.00	254.0	254	506.80	149.60	1098.00	32.00	216.0	216.0	35.0	22.84	29.34
	PA3	41.80	389.00	2.00	1744	2.05	435	2.00	254.0	254	794.40	206.40	1168.00	71.30	219.0	219.0	80.0	25.11	33.99
	PA4	42.20	419.00	2.00	1709	2.05	435	2.00	254.0	254	1146.00	296.80	1152.00	71.30	219.0	219.0	55.0	27.96	37.43
McMullen et al. (1985) [30]	PB1	45.80	435.00	2.00	1638	2.05	310	2.00	178.0	356	285.20	92.80	1099.00	32.00	146.0	324.0	65.0	16.39	22.17
	PB2	45.80	483.00	2.00	1663	2.05	310	2.00	178.0	356	506.80	149.60	1096.00	32.00	140.0	318.0	35.0	18.86	27.54
	PB3	45.50	389.00	2.00	1744	2.05	435	2.00	178.0	356	794.40	206.40	1168.00	71.30	143.0	321.0	85.0	21.80	32.61
	PB4	45.50	419.00	2.00	1709	2.05	435	2.00	178.0	356	1146.00	296.80	1150.00	71.30	143.0	321.0	60.0	24.10	37.60
	PC1	42.20	435.00	2.00	1638	2.05	310	2.00	146.0	438	285.20	92.80	1103.00	32.00	114.0	406.0	75.0	13.92	19.74
	PC2	45.10	483.00	2.00	1663	2.05	310	2.00	146.0	438	506.80	149.60	1090.00	32.00	108.0	400.0	40.0	17.23	28.59
	PC3	41.30	389.00	2.00	1744	2.05	435	2.00	146.0	438	794.40	206.40	1162.00	71.30	111.0	403.0	95.0	18.48	32.78
	PC4	42.10	419.00	2.00	1709	2.05	435	2.00	146.0	438	1146.00	296.80	1149.00	71.30	111.0	403.0	65.0	21.64	38.52
	H3A	92.22	374.00	2.00	1816	1.99	390	2.00	140.0	420	615.75	396.96	1232.41	113.10	98.0	378.0	110.0	19.66	33.32
	H3AR	92.22	487.00	2.00	1816	1.99	390	2.00	140.0	420	804.25	396.96	1229.44	113.10	98.0	378.0	110.0	22.65	33.50
	H2A	91.88	487.00	2.00	1816	1.99	390	2.00	170.0	340	804.25	396.96	1262.41	113.10	128.0	298.0	90.0	15.10	35.78
	H1A	90.66	487.00	2.00	1816	1.99	390	2.00	240.0	240	804.25	396.96	1220.31	113.10	198.0	198.0	85.0	34.68	38.66
	H1AR	94.67	487.00	2.00	1816	1.99	390	2.00	140.0	420	804.25	396.96	946.52	113.10	100.0	380.0	90.0	31.55	38.44
Wafa et al. (1995) [35]	H3B	91.51	374.00	2.00	1841	1.94	387	2.00	140.0	420	615.75	205.56	1135.61	78.54	100.0	380.0	140.0	20.67	26.43
	H2B	95.60	374.00	2.00	1841	1.94	387	2.00	170.0	340	615.75	205.56	1203.46	78.54	130.0	300.0	130.0	27.14	29.46
	H1B	89.78	374.00	2.00	1841	1.94	387	2.00	240.0	240	615.75	205.56	1196.50	78.54	200.0	200.0	120.0	29.88	31.33
	M3A	69.92	487.00	2.00	1816	1.99	390	2.00	140.0	420	804.25	396.96	965.78	113.10	98.0	378.0	110.0	19.57	29.96
	M2A	70.07	487.00	2.00	1816	1.99	390	2.00	170.0	340	804.25	396.96	904.22	113.10	128.0	298.0	100.0	27.00	31.94
	M1A	72.54	487.00	2.00	1816	1.99	390	2.00	240.0	240	804.25	396.96	934.46	113.10	198.0	198.0	90.0	31.46	35.41
	M3B	69.33	374.00	2.00	1841	1.94	387	2.00	140.0	420	615.75	205.56	923.93	78.54	100.0	380.0	140.0	18.30	24.52
	M2B	69.67	374.00	2.00	1841	1.94	387	2.00	170.0	340	615.75	205.56	925.09	78.54	130.0	300.0	130.0	-	26.17
	M1B	71.97	374.00	2.00	1841	1.94	387	2.00	240.0	240	615.75	205.56	888.27	78.54	200.0	200.0	120.0	26.81	28.94

Table 1. *Cont.*

| Author	Beam Name	f_{ck} (MPa)	f_{ly} (MPa)	E_{sl} (MPa, ×10⁵)	f_{py} (MPa)	E_{ps} (MPa, ×10⁵)	f_{ty} (MPa)	E_{st} (MPa, ×10⁵)	B (mm)	H (mm)	A_l (mm²)	A_{ps} (mm²)	f_{pe} (Mpa)	A_t (mm²)	x_0 (mm)	y_0 (mm)	s (mm)	T_{cr} (kNm)	T_u (kNm)
Ashour et al. (1999) [33]	H2B	95.60	374.00	2.00	1841	1.94	387	2.00	170.0	340	615.75	205.56	1203.46	78.54	130.0	300.0	130.0	-	28.46
	H2A	91.88	487.00	2.00	1816	1.99	390	2.00	170.0	340	804.25	396.96	1262.41	113.10	128.0	298.0	100.0	-	35.78
Allos et.al. (1989) [32]	A2	41.04	0.00	0.00	1430	2.09	408	2.00	100.0	175	0.00	157.08	2057.49	28.27	69.0	144.0	80.0	-	4.03
	C1	41.04	0.00	0.00	1430	2.09	408	2.00	100.0	175	0.00	157.08	2057.49	28.27	69.0	144.0	50.0	-	4.15
	C2	41.04	0.00	0.00	1430	2.09	408	2.00	100.0	175	0.00	157.08	2057.49	28.27	69.0	144.0	80.0	-	3.95
	C3	41.04	0.00	0.00	1430	2.09	408	2.00	100.0	175	0.00	157.08	2057.49	28.27	69.0	144.0	100.0	-	3.84
Jeng et al. (2018) [36]	A09	46.70	455.00	1.98	1860	2.00	455	1.98	400.0	617	1290.00	991.20	1044.00	129.00	347.3	564.3	130.0	133.63	224.66
	A19	52.20	366.00	2.00	1860	2.00	445	1.98	350.0	465	426.00	1843.40	840.00	129.00	297.3	412.3	200.0	109.60	137.72
	B17	71.60	398.00	2.00	1860	2.00	454	2.00	298.0	450	426.00	1831.70	858.00	129.00	245.3	397.3	180.0	91.02	109.66
	B20	71.70	500.00	1.92	1860	2.00	534	1.98	271.0	453	710.00	1829.10	894.00	129.00	218.3	400.3	110.0	79.39	122.64
	C12-1	85.20	500.00	1.92	1860	2.00	534	1.98	252.0	448	426.00	984.90	1079.00	129.00	199.3	395.3	160.0	59.88	83.83
	C12-2	88.40	460.00	2.01	1860	2.00	458	1.94	320.0	459	774.00	1702.80	879.00	129.00	267.3	406.3	280.0	97.03	106.33
	A08-D	54.40	455.00	1.94	1860	2.00	464	1.99	398.0	608	1290.00	851.40	1151.00	129.00	345.3	555.3	130.0	149.82	232.58

Note: * hollow section, and ** eccentricity of the prestressing tendon by 0.156 of e/d.
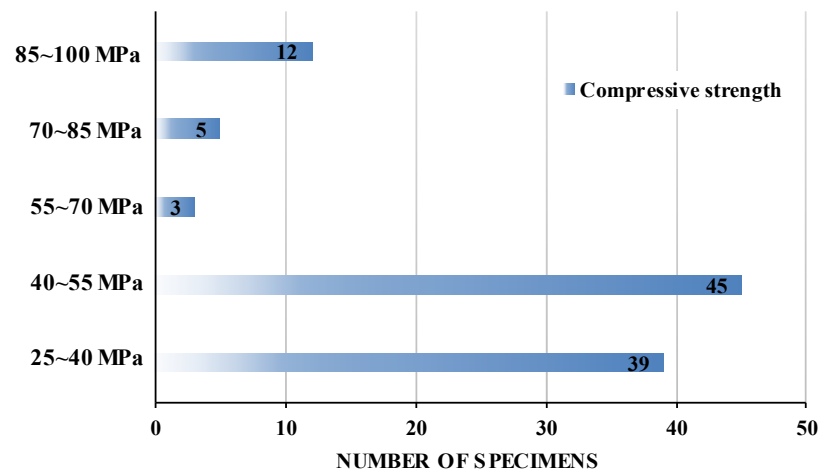
(**a**)
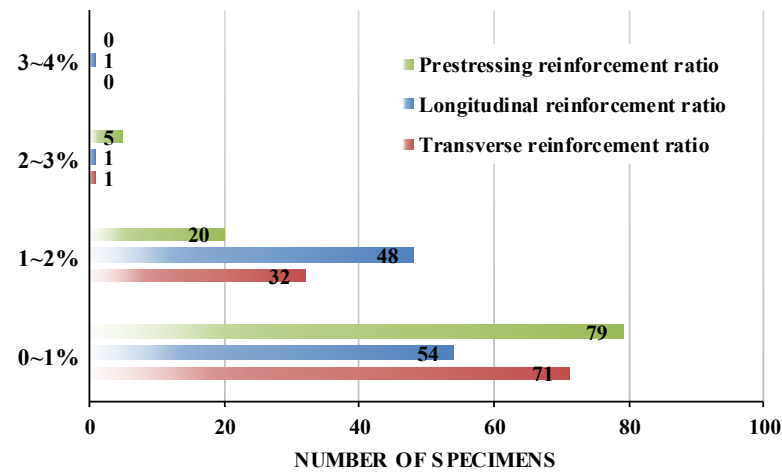
(**b**)
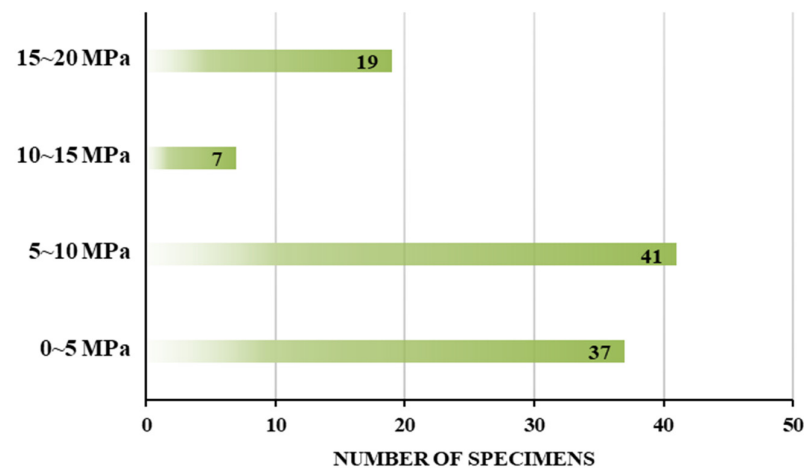
(**c**)

Figure 6. Distribution of the key parameters in the specimens: (**a**) compressive strength of concrete; (**b**) reinforcement ratios; (**c**) compressive stress at the concrete section due to prestress.

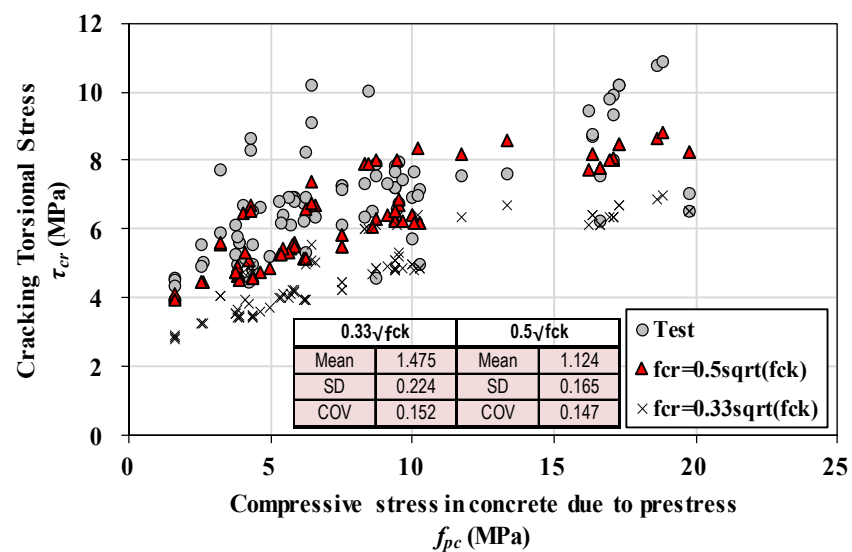The torsional capacity of the specimens was evaluated through the torsional shear stress, which was defined as the cracking torsional shear stress (τ_{cr}) and ultimate torsional shear stress, according to ACI 318-19 [29].

$$\tau_{cr,ACI} = \frac{T_{cr}p_{cp}}{A_c^2} \tag{28}$$

$$\tau_{u,ACI} = \frac{T_u p_h}{1.7 A_{oh}^2} \tag{29}$$

$\tau_{cr,ACI}$ was derived from the relationship in Equation (1) by applying the thickness ($t_d = 0.75 A_c/p_{cp}$) prior to cracking and the perimeter area ($A_o = (2/3)A_c$) specified in ACI 318-19. Here, A_{oh} represents the cross-sectional area close to the centerline of the outermost torsional reinforcement. In addition, T denotes the torsional moment. The torsional shear stresses according to f_{pc} are plotted in Figure 7 using the cracking torsional moment and ultimate torsional moment from the experimental results reported in the literature. The cracking torsional capacity is enhanced by prestress, and the ultimate torsional strength tends to increase owing to f_{pc}. Therefore, the effect of prestress should also be considered when evaluating the torsional strength.

(a)
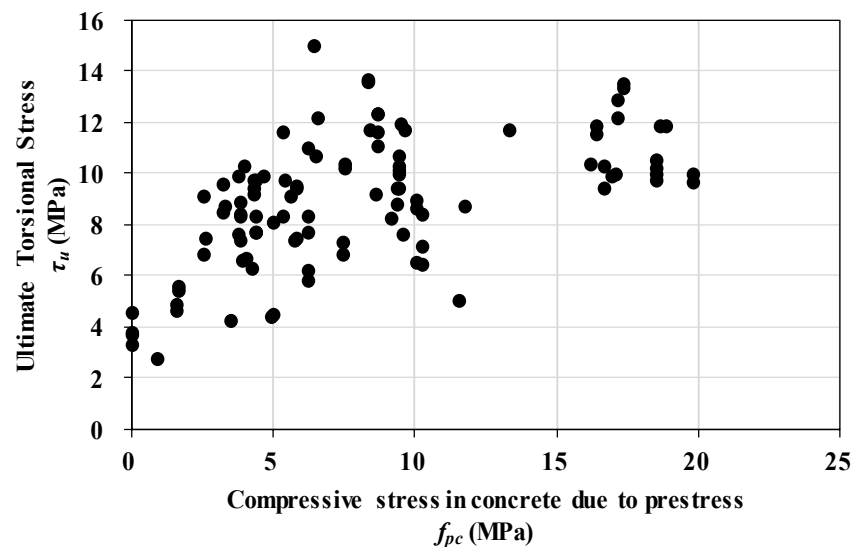
(b)

Figure 7. Torsional shear stress of the specimens: (**a**) cracking torsional shear stress; (**b**) ultimate torsional shear stress.

The evaluation of the cracking shear stress through Equation (16) shows that the tendency of the torsional capacity to increase with f_{pc} is well estimated but somewhat conservative. According to Ju et al. [39], the cracking torsional strength of reinforced concrete beams is 1.5 times that estimated by Equation (16). In addition, they suggested the use of $0.5\sqrt{f_{ck}}$ instead of $0.33\sqrt{f_{ck}}$ for f_{cr}. Figure 7a shows that the use of $0.5\sqrt{f_{ck}}$ for f_{cr} evaluates the cracking torsional shear stress with good accuracy, with a mean of 1.124 and a coefficient of variation (COV) of 0.147. However, for the torsional strength of prestressed concrete beams proposed in this study, Equation (16) with $0.33\sqrt{f_{ck}}$ for f_{cr} is used to evaluate the torsional strength to be on the conservative side.

3.2. Torsional Strength Model Specified in ACI 318-19

The torsion model specified in the design code was applied to the collected specimens to evaluate the accuracy of the model and to compare it with that of the proposed model in terms of torsional strength. The design codes for structural concrete used in North America and Europe adopt a torsional design model based on the thin-walled tube theory and the space truss model [40] in common. Although details such as the definition of the effective thickness of the thin-walled tube (t_d), angle of the compression diagonal (θ), and maximum torsional strength limit are somewhat different in each standard, they essentially present the same torsional strength calculation formula based on the truss model. Therefore, for the torsional strength calculation model presented in ACI 318-19 [29], the current American concrete structural design standard was used to evaluate the torsional strength of the prestressed concrete beams collected from the literature.

The torsional design model in ACI 318 suggests that the nominal torsional strength of reinforced concrete beams is based on the resistance of the closed stirrups. However, to satisfy the force equilibrium with the longitudinal reinforcement, the torsional strength is determined as follows:

$$T_{n,ACI} = min\left(\frac{2A_o A_t f_{ty}}{s}cot\theta, \frac{2A_o\left(A_l f_{ly} + A_p f_{py}\right)}{p_h}tan\theta\right) \tag{30}$$

where A_o is the cross-sectional area close to the centerline of the shear flow ($= 0.85A_{oh}$), θ is the compression diagonal angle according to the truss analogy in the torsional analysis, p_h is the perimeter of the centerline of the outermost transverse closed stirrup, and f_{py} is the yield strength of the prestressing tendon. The compressive strength of the concrete (f_{ck}) was limited according to $\sqrt{f_{ck}} \leq 8.3$ MPa, and the yield strengths of the longitudinal reinforcement and stirrups were limited to 420 MPa. In addition, the torsional strength was limited to $(5/6)\sqrt{f_{ck}}1.7A_{oh}^2/p_h$. The compressive diagonal angle (θ) was calculated from the equilibrium relationship between the forces in the longitudinal reinforcement and stirrups, assuming yielding of the reinforcement in both directions, as follows:

$$\theta = cot^{-1}\left(\sqrt{\frac{A_l f_{ly} + A_p f_{py}}{A_t f_{ty}}\frac{s}{p_h}}\right) \tag{31}$$

where θ should not be less than 30° or greater than 60°. However, for design purposes, 45° is permitted for use by non-prestressed members or members with less than 40% of the tensile forces of the reinforcing steel plus prestressing tendons and 37.5° for prestressed members or members with greater than 40% of the tensile forces of the reinforcement.

3.3. Contributions of Tube End Reinforcements

Figure 8 shows the torsional strength evaluation results of the prestressed concrete beams according to f_{pc}. The torsional strength of the prestressed concrete beams was estimated by the proposed model with good accuracy, with a mean value of 1.123 and a COV of 17.7% in terms of the ratio of the experimental to the estimated torsional strength. Figure 8a shows the results of applying the proposed model using $f_{cr} = 0.5\sqrt{f_{ck}}$ to

Equation (16). In this case, the mean improved to 1.023, but the COV increased to 19.3%, and a significant number of specimens were deemed unsafe. In addition, as shown in Figure 8b, if the effect of prestress was not considered, the proposed model not only underestimated the torsional strength of the specimens with a mean of 1.691 but also provided a somewhat higher scatter with a COV of 30.5%.

(a)

(b)
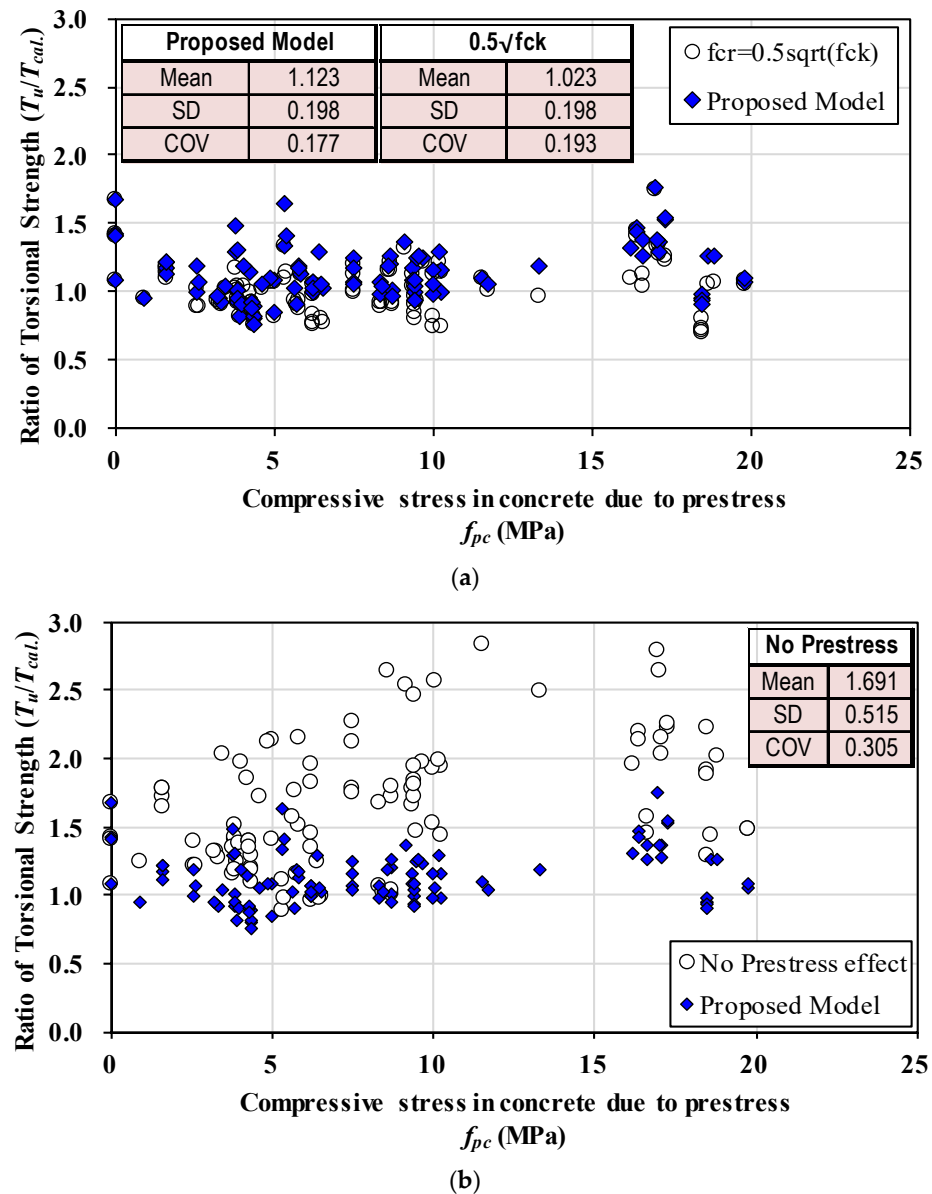
Figure 8. Torsional strength estimated by the proposed model: (**a**) according to cracking; (**b**) according to the prestress effect.

To compare the accuracy of the proposed model, the torsional strength estimation results obtained using the ACI 318-19 method are shown in Figure 9. The torsional strength of ACI 318-19 was calculated using Equation (30), and the strength was determined by the reinforcement in the direction in which the yielding of the reinforcement occurred first, considering the equilibrium of the longitudinal and transverse reinforcements. In addition, the compressive diagonal angle (θ) limit was considered. Figure 9a shows the torsional strength of the beams with angle limits, whereas Figure 9b shows the estimation results without angle limits, reflecting the fact that prestressed concrete members have lower compressive diagonal angles than nonprestressed concrete beams. In addition, ACI 318

provides the compressive diagonal angle as 45° for nonprestressed members and 37.5° for prestressed concrete members. Based on this suggestion, the torsional strength estimated with a fixed angle of 37.5° for θ is presented in Figure 9c.

(a)

(b)

(c)
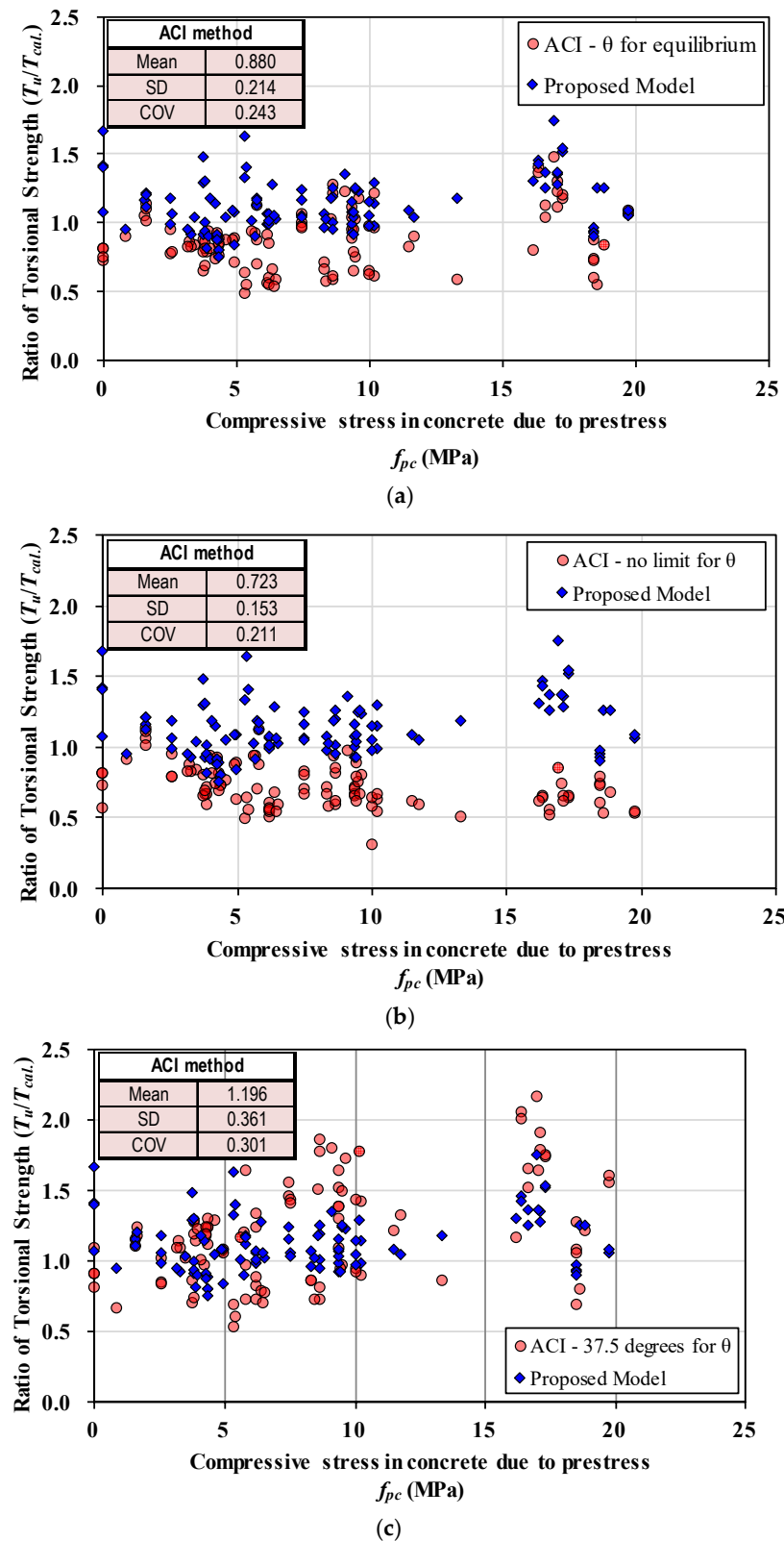
Figure 9. Comparison of the estimations with ACI 318: (**a**) limited θ in the ACI model for equilibrium; (**b**) unlimited θ in the ACI model for equilibrium; (**c**) θ of 37.5 degrees in the ACI model.

As shown in Figure 9a,b, ACI 318 tended to overestimate the torsional strength, especially when the limit of the compression diagonal angle (θ) was not considered. The accuracy improved slightly; however, several specimens were estimated on the unsafe side with a mean of 0.723 in terms of $T_{exp.}/T_{cal.}$. However, when a fixed θ of 37.5° was used, the specimens were estimated on the safe side, and the mean value of $T_{exp.}/T_{cal.}$ was 1.123, as shown in Figure 9c. In this case, the compression diagonal angle (θ) needed to satisfy the force equilibrium with the prestress was calculated to be lower than 37.5° for most of the specimens using Equation (31). In all the cases, the torsional strength was determined by the yield strength of the transverse torsional reinforcement.

CSA, a Canadian standard, has been reported to be somewhat more accurate in estimating the torsional strength of reinforced concrete beams than ACI 318, and EC2, a European standard, which provides significantly more conservative results [41]. Despite some differences in the determination of key variables, the aforementioned design standards have similar accuracy because they are all based on the truss and thin-walled tube models used to calculate the torsional strength by disregarding the contribution of concrete. Therefore, the contribution of concrete to the torsional strength due to prestress was not accurately considered, and the proposed model presented in this study was able to accurately evaluate the effect of prestress while calculating the torsional strength on the conservative side.

As a result, the proposed model well estimated the torsional strength of prestressed concrete beams regardless of the torsional cracking strength applied to the model. Also, the estimation accuracy of the proposed model was much higher than that of the ACI 318-19 method. Moreover, the proposed torsional strength model showed a clear effect of prestress in terms of the ultimate torsional strength that increased up to 50% for the prestressing level ranging from 1 to 19.75 MPa.

4. Conclusions

In this study, a model for estimating the strength of prestressed concrete beams subjected to a pure torsional moment is presented by extending the multipotential capacity model. In this model, the effect of axial stress induced by effective prestress was incorporated into the shear element analysis of reinforced concrete members subjected to torsional loading, and the torsional strength model was verified using 104 specimens collected from the existing literature. The conclusions drawn from this study are summarized as follows.

(1) Assuming the principal tensile stress and principal compressive strain to be zero in the shear element of a reinforced concrete member subjected to torsion in the ultimate state, and a torsional strength model was derived by simplifying the force equilibrium and strain compatibility conditions.

(2) In the derivation of the torsional strength model, the effects of the initial crack angle, principal stress angle, longitudinal strain, and torsional effective thickness in the shear element were considered, considering the effective prestress acting on the prestressed concrete member.

(3) Based on the multipotential capacity criteria, the failure mode was categorized into a compressive failure of concrete and aggregate interlocking failure at the crack surface, and the effect of prestress was reflected in the crack width calculation formula to determine the aggregate interlocking in a rational manner.

(4) The results of the torsional strength evaluation that included the effect of prestress show a mean value of 1.123 for the experimental-to-calculated ratio and a COV of 17.7% for the 104 specimens collected from the literature, showing better accuracy than the estimation results without considering prestress, which had a mean of 1.691 and a COV of 30.5%.

(5) The torsional strength of the experimental specimens was evaluated according to the ACI 318-19 with a mean of 0.880 and COV of 24.3%, which is less accurate than the proposed model and significantly unsafe. When the compressive diagonal angle of prestressed concrete beams was set to 37.5° according to ACI 318, the torsional strength

of the specimens was evaluated with improved accuracy, with a mean of 1.196 and COV of 30.1%.

(6) The proposed model reasonably reflects the influence of prestress and evaluates the strength of prestressed concrete beams subjected to a pure torsional moment with good accuracy. However, this study intended to provide some insight into the torsional behavior of prestressed concrete beams, and there is seldom pure torsion for box girders in real practice. Thus, this model is expected to be extended to the strength evaluation model of prestressed concrete beams resisting torsional moment in combination with bending moment, shear force, and axial force in the future.

Author Contributions: Conceptualization, methodology, writing—original draft preparation, and supervision, H.J.; investigation and data curation and validation, C.J.; writing—review and editing and funding acquisition, H.-C.C. All authors have read and agreed to the published version of the manuscript.

Data Availability Statement: The original contributions presented in the study are included in the article, further inquiries can be directed to the corresponding author/s.

Conflicts of Interest: Author Hae-Chang Cho was employed by the company Technology Center, Dream Structural Engineers Co., Ltd. The remaining authors declare that the research was conducted in the absence of any commercial or financial relationships that could be construed as a potential conflict of interest.

References

1. Ju, H.; Lee, D.H.; Hwang, J.H.; Kang, J.W.; Kim, J.S.; Oh, Y.H. Torsional Behavior Model of Steel Fiber-Reinforced Concrete Members Modifying Fixed-Angle Softened-Truss Model. *Compos. Part B Eng.* **2013**, *45*, 215–231. [CrossRef]
2. Ju, H.; Lee, D.H.; Hwang, J.H.; Kim, K.S.; Oh, Y.H. Fixed-Angle Smeared-Truss Approach with Direct Tension Force Transfer Model for Torsional Behavior of Steel Fiber-Reinforced Concrete Members. *J. Adv. Concr. Technol.* **2013**, *11*, 215–229. [CrossRef]
3. Ju, H.; Lee, D.; Zhang, W.; Wang, L. Torsional Strength Model of Reinforced Concrete Members Subjected to Combined Loads. *Comput. Concr.* **2022**, *29*, 285–301.
4. Han, S.J.; Ju, H.; Joo, H.E.; Kim, K.S. Shear resistance mechanism of prefabricated large-scale gerber girder. *J. Build. Eng.* **2024**, *83*, 108424. [CrossRef]
5. Meiramov, D.; Seo, Y.; Ju, H.; Cho, H.C. Direct Tensile Capacity of Steel Tube Connections in Precast Concrete Double-Wall System. *Building* **2023**, *13*, 2872. [CrossRef]
6. Ju, H.; Han, S.J.; Choi, I.S.; Choi, S.; Park, M.K.; Kim, K.S. Experimental Study on Optimized-Section Precast Slab with Structural Aesthetics. *Appl. Sci.* **2018**, *8*, 123. [CrossRef]
7. Ju, H.; Kim, K.S.; Lee, D.H.; Hwang, J.H.; Choi, S.H.; Oh, Y.H. Torsional Responses of Steel Fiber-Reinforced Concrete Members. *Compos. Struct.* **2015**, *129*, 143–156. [CrossRef]
8. Ju, H.; Han, S.J.; Kim, K.S. Analytical Model for Torsional Behavior of RC Members Combined with Bending, Shear, and Axial Loads. *J. Build. Eng.* **2020**, *32*, 101730. [CrossRef]
9. Ju, H.; Lee, D. Nonlinear Analysis of RC Members Subjected to Combined Torsion and Bending Moment. *ACI Struct. J.* **2021**, *118*, 55–70.
10. Kryzhanovskiy, K.; Zhang, D.; Ju, H.; Kim, J. Development of Torsional Strength Model for Steel Fiber Reinforced Concrete Beams with Transverse Reinforcement. *Int. J. Civ. Eng.* **2023**, *21*, 1123–1139. [CrossRef]
11. Bredt, R. Kritische Bemerkungen zur Drehungselastizitat. *Z Vereines Deutscher Ingenieure. Band* **1896**, *40*, 785–790.
12. Hsu, T.T.C.; Zhang, L.X. Nonlinear analysis of membrane elements by fixed-angle softened-truss model. *ACI Struct. J.* **1997**, *94*, 483–492.
13. Hsu, T.T.C.; Mo, Y.L. *Unified Theory of Concrete Structures*; Wiley and Sons: Hoboken, NJ, USA, 2010.
14. Rahal, K.N.; Collins, M.P. Effect of Thickness of Concrete Cover on Shear-Torsion Interaction—An Experimental Investigation. *ACI Struct. J.* **1995**, *92*, 334–342.
15. Greene, G.G.; Belarbi, A. Model for Reinforced Concrete Members under Torsion, Bending, and Shear. I: Theory. *J. Eng. Mech.* **2009**, *135*, 961–969. [CrossRef]
16. Mitchell, D.; Collins, M.P. Diagonal compression field theory—A rational model for structural concrete in pure torsion. *ACI J.* **1974**, *71*, 396–408.
17. Bentz, E.C.; Collins, M.P. Development of the 2004 Canadian Standards Association (CSA) A23.3 Shear Provisions for Reinforced Concrete. *Can. J. Civ. Eng.* **2006**, *33*, 521–534. [CrossRef]

18. Vecchio, F.J.; Collins, M.P. Modified Compression Field Theory for Concrete Elements Subjected to Shear. *ACI J.* **1986**, *83*, 219–231.

19. Haddadin, M.J.; Hong, S.T.; Mattock, A.H. Stirrup Effectiveness in Reinforced Concrete Beams with Axial Force. *Proc. Am. Soc. Civ. Eng.* **1971**, *97*, 2277–2297. [CrossRef]

20. Park, R.; Paulay, T. *Reinforced Concrete Structures*; Wiley: New York, NY, USA, 1975.

21. Ju, H.; Han, S.J.; Kim, K.S.; Strauss, A.; Wu, W. Multi-Potential Capacity for Reinforced Concrete Members under Pure torsion. *Struct. Eng. Mech.* **2020**, *75*, 401–414.

22. Hsu, T.T.C. *Torsion of Reinforced Concrete*; Van Nostrand Reinhold, Inc.: New York, NY, USA, 1984.

23. Hsu, T.T.C.; Mo, Y.L. Softening of concrete in torsional members—Theory and Tests. *ACI J.* **1985**, *82*, 290–303.

24. Hsu, T.T.C.; Mo, Y.L. Softening of concrete in torsional members—Prestressed Concrete. *ACI J.* **1985**, *82*, 603–615.

25. Lee, J.Y.; Kim, K.H.; Kim, S.W. Non-linear shear analysis of reinforced concrete columns by fixed-angle theory. *Proc. Inst. Civil Eng. Struc. Build.* **2013**, *166*, 165–181. [CrossRef]

26. Voo, J.Y.L.; Foster, S.J. *Variable Engagement Model for Fiber Reinforced Concrete in Tension*; UNICIV Report No. R-420; University of New South Wales: Sydney, Australia, 2003.

27. Lee, J.Y.; Kim, S.W. Torsional strength of RC beams considering tension stiffening effect. *J. Struct. Eng.* **2010**, *136*, 1367–1378. [CrossRef]

28. Jeng, C.H.; Hsu, T.T.C. A Softened Membrane Model for Torsion in Reinforced Concrete Members. *Eng. Struct.* **2009**, *32*, 1944–1954. [CrossRef]

29. *ACI 318-19*; ACI Committee 318, Building Code Requirements for Structural Concrete (ACI 318-19). American Concrete Institute: Farmington Hills, MI, USA, 2019.

30. McMullen, A.E.; EI-Degwy, W.M. Prestressed Concrete Tests Compared with Torsion Theories. *PCI J.* **1985**, *30*, 96–127. [CrossRef]

31. Rahal, K.N. Evaluation of AASHTO-LRFD General Procedure for Torsion and Combined Loading. *ACI Struct. J.* **2006**, *103*, 683–692.

32. Allos, A.E.; Rashid, A.H. Prestressed Concrete Rectangular Beams Subjected to Sustained Torque. *ACI Struct. J.* **1989**, *86*, 469–472.

33. Ashour, S.A.; Shihata, S.A.; Akhtaruzaman, A.A.; Wafa, F.F. Prestressed high-strength concrete beams under torsion and bending. *Can. J. Civ. Eng.* **1999**, *26*, 197–207. [CrossRef]

34. Chander, H. Behavior of Prestressed Concrete Rectangular Members Subjected to Pure Torsion. Doctoral Dissertation, West Virginia University, Morgantown, WV, USA, 1970.

35. Wafa, F.F.; Shihata, S.A.; Ashour, S.A.; Akhtaruzzaman, A.A. Prestressed high-strength concrete beams under torsion. *J. Struct. Eng.* **1995**, *121*, 1280–1286. [CrossRef]

36. Jeng, C.H.; Chao, M. Torsion Experiment and Cracking-Torque Formulas of Prestressed Concrete Beams. *ACI Struct. J.* **2018**, *115*, 1267–1278. [CrossRef]

37. Mitchell, D.; Collins, M.P. The Behaviour of Structural Concrete Beams in Pure Torsion; Publication No. 74-06. Ph.D. Thesis, Department of Civil Engineering, University of Toronto, Toronto, ON, USA, 1974.

38. Mukherjee, P.R. Ultimate Torsional Strength Of Plain, Prestressed And Reinforced Concrete members Of Rectangular Cross-Section. Ph.D. Thesis, West Virginia University, Morgantown, WV, USA, 1967.

39. Ju, H.; Han, S.J.; Zhang, D.; Kim, J.; Wu, W.; Kim, K.S. Estimation on Minimum Torsional Reinforcement of Reinforced Concrete and Steel Fiber Reinforced Concrete Members. *Adv. Mater. Sci. Eng.* **2019**, *2019*, 4595363. [CrossRef]

40. Joint ACI-ASCE Committee 445. *445.1R-12 Report on Torsion in Structural Concrete*; American Concrete Institute: Farmington Hills, MI, USA, 2013.

41. Ju, H.; Lee, D.; Kim, K.H.; Yerzhanov, M.; Zhang, D.; Kim, J.R. Torsional Design Method Used in Eurasia Region: A Comparative Study. *Struct. Concr.* **2021**, *22*, 3798–3834. [CrossRef]